

Effect of Curing Conditions and BaTiO₃ Nanoparticle Addition on Dielectric Constant of PDMS for EAP Applications

B.S. AKDEMIR^{a,b,*} AND I.M. KUSOGLU^{b,c}

^aGebze Technical University, Department of Nanoscience and Nanoengineering, Kocaeli, Turkey

^bDokuz Eylül University, Department of Nanoscience and Nanoengineering, İzmir, Turkey

^cDuisburg-Essen Universität, Technical Chemistry I, Duisburg, Germany

Received: 10.11.2020 & Accepted: 01.02.2021

Doi: [10.12693/APhysPolA.139.145](https://doi.org/10.12693/APhysPolA.139.145)

*e-mail: solenakdemir@gmail.com

To a great extent, dielectric properties of electroactive polymers affect actuator efficiency. In this study, we examined the effect of BaTiO₃ nanoparticles addition on dielectric constant of a PDMS nanocomposite. We optimized the curing conditions of PDMS for the highest dielectric constant. After that, we added several amounts of BaTiO₃ nanoparticles (0.5–30 wt%) to PDMS. Dielectric constants of the samples were calculated by measuring capacitance values by an LCR meter at 10 kHz. The highest dielectric constant (5.09×10^{-25}) belonged to the PDMS which was cured at 100°C for 35 min. Structural properties of PDMS and BaTiO₃ nanoparticles were determined by the Fourier transform infrared spectroscopy, differential thermal analysis, X-ray diffraction and scanning electron microscopy.

topics: electroactive polymer composite, piezoelectric nanoparticle, BaTiO₃, PDMS

1. Introduction

As technology improves, new devices are developed and used in our everyday lives. State-of-the-art technological devices require new energy systems such as smaller, lighter and more effective actuators. Conventional actuators (electromotors and combustion engines [1]) cannot provide this energy. A solution would be to combine smart materials with actuator systems to develop a new kind of actuators.

Smart materials are one of the candidates for effective actuators. They respond to an external stimulus in real time or near real time [2, 3] in a repeatable, reversible, fast and significant way [4]. They change one or more of their physical properties according to such visible and measurable external energies like temperature, pH, light, and magnetic and electric field in a controllable way [2–9].

Electroactive polymers (EAPs) exhibit considerable stress and/or strain upon electrical stimulation with a change in shape or size [2–9]. They create a motion as actuators like torque generation in conventional electric motors [3]. They are smart and high performance actuators [6–9]. Electroactive polymers are favored in high technology applications because they have good electromechanical properties, large actuation strain, comparatively low actuation stress [4], flexible behavior and high efficiency at small scales [3] as well as they easily processable, light weight and low cost [3, 4, 9, 10].

The EAP materials should have high deformability and dielectric behavior to convert energy into different forms for clean energy [11]. Silicones are dielectric materials which deform reversibly and this makes them the best candidates for energy conversion. However, their low dielectric properties are their main disadvantage.

There are many studies reported on improving dielectric properties of silicones and mostly ceramic fillers which have a high dielectric constant, like barium titanate (BaTiO₃) [12], are added to them. In such studies, Nayak et al. used a BaTiO₃/PDMS composite having filler ratios of 0–70 per hundred parts mixed by an internal mixer [13]. Bele et al. mechanically mixed BaTiO₃ in ratios of 0–15 wt% with PDMS [12]. Xie et al., in turn, studied a polyimide/BaTiO₃ composite obtained through chemical processes [11] while Yaqoob et al. examined a P(VDF-TrFE)/BaTiO₃/MWCNT composite by adding conductive fillers during a polymer synthesis [14]. Further, Stefanescu et al. used fiberglass PMMA with both the neat BaTiO₃ particles and the PEDOT:PSS surface treated BaTiO₃ particles to observe the difference in dielectric constant [15]. In all studies mentioned above, BaTiO₃ was used in a particle form but some researchers used nanowires to examine the shape effect on dielectric constant. All the research groups found that the dielectric constant increases with increasing filler content, surface treatment and shape effect [16].

Barium titanate has high dielectric properties due to a perovskite structure and eco-friendly behavior, unlike lead-based piezoelectric materials [17]. Consequently, in this study, we used BaTiO₃ as a conductive filler content (0.5–30 wt%) in a polymer matrix.

2. Experimental procedure

Silicon elastomer PDMS (polydimethylsiloxane) is synthesized from a kit (Sylgard 184, Dowsil) containing a polymer base and a crosslinking agent. First, the polymer base was poured into a beaker and then a curing agent was added in a ratio of 10:1, and stirred manually. The stirred mixture was poured into a metal mold with cavities of 20 mm length, 5 mm width and 500 μ m depth to form bulk samples. Air bubbles formed during stirring were deaerated under vacuum at 700 mm Hg for 15 min with a cold molding vacuum device. As shown in Table I, PDMS was cured at several temperatures and durations to obtain the highest dielectric constant. Barium titanate nanoparticles (Nanografi, Ankara) with particle size lower than 300 nm were used. The differential thermal analysis (DTA), Fourier transform infrared spectroscopy (FTIR) and X-ray diffraction (XRD) measurements were made on the as-received particles. All results were supported by the literature [18–22]. All other chemicals were purchased from local companies.

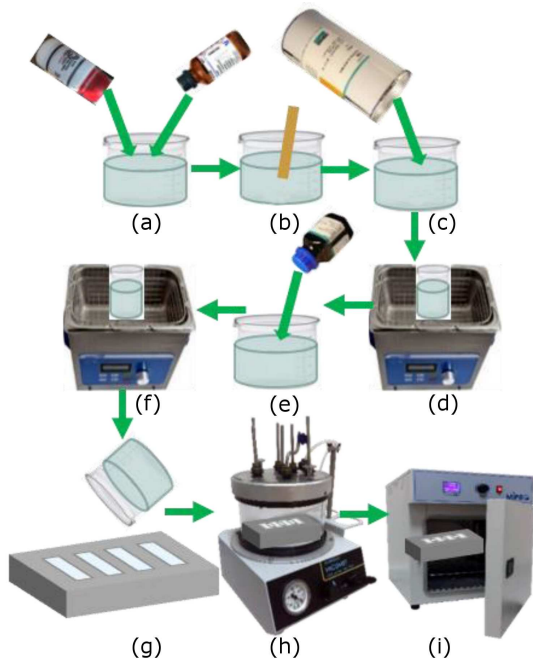


Fig. 1. Production of PDMS-BaTiO₃ nanocomposites: (a) BaTiO₃-toluene mixing, (b) manual stirring, (c) PDMS adding, (d) ultrasonication, (e) curing agent adding, (f) ultrasonication, (g) casting, (h) deaeration, (i) curing [24].

Curing conditions of PDMS. TABLE I

Sample code	Temperature [°C]	Time
P25/24	25	24 h
P40/4	40	4 h
P40/6	40	6 h
P60/3	60	3 h
P60/4	60	4 h
P80/1	80	1 h
P80/2	80	2 h
P80/3	80	3 h
P100/35	100 ^a	35 min
P125/20	125 ^a	20 min
P150/10	150 ^a	10 min

^a From technical data sheet of PDMS [23]

To produce PDMS-BaTiO₃ nanocomposites, BaTiO₃ nanoparticles were dispersed in 25 wt% toluene by stirring manually for 5 min. Then, the PDMS base was added. The mixture was put into an ultrasonic mixer for 60 min. After mixing, the curing agent was added and ultrasonicated for 10 min. Then, the same procedures as in the PDMS production were carried out (casting into a metal mold and deaeration). Finally, the deaerated samples were cured at a specified temperature during a specified time (see Fig. 1).

For morphological examinations, a COXEM EM-30 Plus scanning electron microscopy was used in both the secondary electron image (SEI) and backscattered electron image (BEC) modes. To get information about bonding types, FTIR analyses were made by using Thermo Scientific NICOLET iS10. Thermogravimetric analyses were performed by Perkin Elmer STA 6000. Further, a ViTiny UM12 digital microscope was used to obtain high magnification optical images and dimensional measurement. Dielectric constant calculations were made by measuring capacitance values obtained by a HIOKI LCR meter.

3. Results and discussion

3.1. Effect of curing conditions on dielectric constant of PDMS

The PDMS was cured at several temperatures (25–150°C) and several durations (10 min–24 h) to optimize the curing conditions [25–29]. The given sample codes for curing conditions of PDMS are given in Table I.

For the graphs, we used “10035” abbreviation to describe the curing of PDMS at 100°C for 35 min to make it easier. According to these, the dielectric constant values of various samples cured at different conditions are given in Fig. 2. The points indicate the average values of six capacitance measurements.

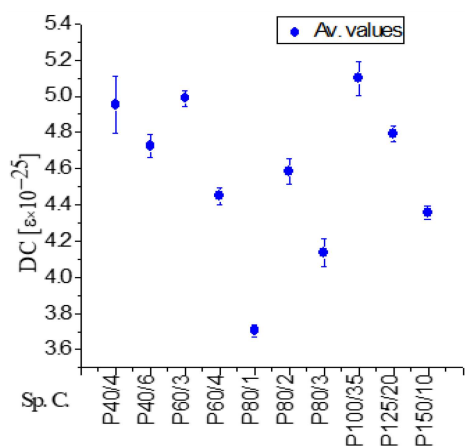


Fig. 2. Dielectric constants of samples cured at different conditions. Dielectric constant is denoted as “DC”, the sample code — “Sp. C.” and average values — “Av. values”.

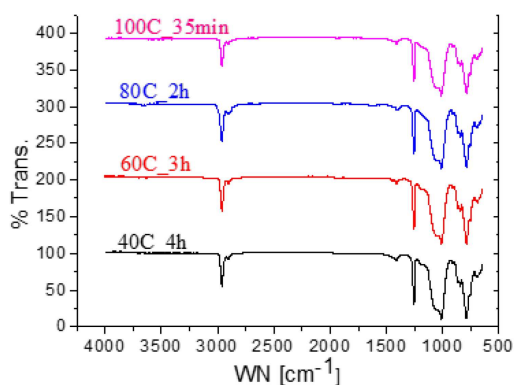


Fig. 3. FTIR results of samples cured at different temperatures and times. Transmittance is denoted as “Trans.” and wave number — “WN”.

Standard deviations are shown in the graph as error bars. The highest dielectric constant was obtained at 100°C during a 35-min curing condition. The dielectric constant is high at the high curing temperature since the cross-linking reactions negatively affect the dielectric constant. At low temperatures — because of the slow cross-linking reaction at the beginning of the process — the dielectric constant becomes smaller [30]. After setup optimization, the curing condition was held at 100°C and 35 min because of the highest dielectric constant.

The FTIR results of different curing parameters were analyzed as shown in Fig. 3. To compare FTIR data, we chose only the samples which have the highest dielectric constant in each curing temperature. We found no significant effect of the curing temperature and duration on the bonding properties. The peaks describe transmittance values of different bonding types at a specified wave number shown in Fig. 3. At 2962 cm⁻¹, the peak belongs to C-H stretching in CH₃. The CH₃ symmetric and asymmetric bending in Si-CH₃ is related with

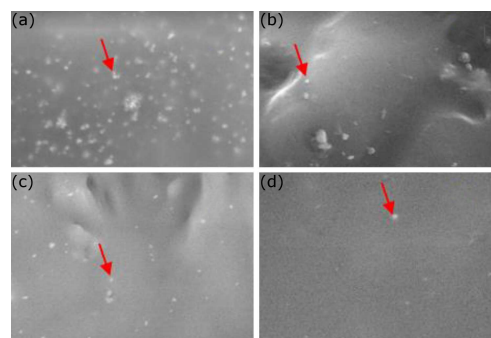


Fig. 4. SEM images: (a) 40C_4h (×10k SEI), (b) 60C_3h (×10k SEI), (c) 80C_1h (×10k BEC), (d) 100C_35min (×10k BEC). The white dots indicated with red arrows represent BaTiO₃ nanoparticles and light gray matrix represents PDMS.

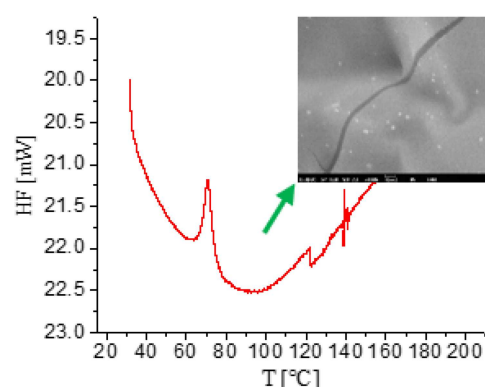


Fig. 5. DTA graph of 80C_1h sample; inset: SEM image of 80C_1h sample. Heat flow endo down is denoted as “HF” and temperature — “T”.

the peak at 1445, 1412, and 1257 cm⁻¹. The peak at around 1050 cm⁻¹ is related with the Si-O-Si bonds. The peaks between 800 and 600 cm⁻¹ are related with the CH₃ rocking in Si-CH absorption [21, 22].

According to these results, SEM analyses were made to observe the surface morphology. The SEM images of samples which were cured at 40, 60, 80, and 100°C are shown in Fig. 4. As shown in the figure, sample surfaces were smooth and there was no formation of observable cracks except for 80C_1h sample shown in the inset of Fig. 5. The reason for that is that at 70°C, there is an exothermic peak in the DTA result related with the outgassing shown in Fig. 5.

3.2. Effect of BaTiO₃ addition on dielectric constant of PDMS nanocomposites

We prepared several ratios to examine the BaTiO₃ addition effect on the PDMS matrix. In the main text, we use labels to define our samples as “curing temperature_curing time_particle content.” For example, 100C_35min_0.5B means that the sample contains 0.5 wt% BaTiO₃ and is cured at 100°C during 35 min.

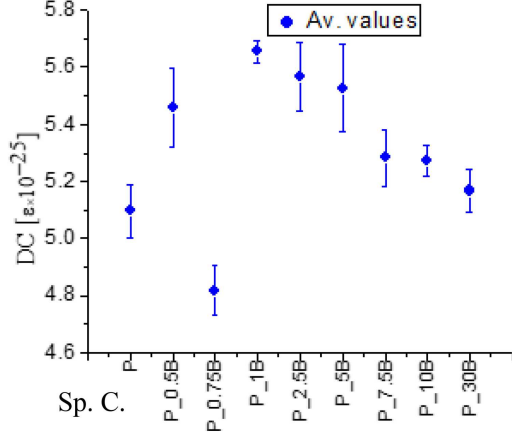


Fig. 6. Dielectric constants of samples containing different amounts of BaTiO₃ additives.

TABLE II

Sample codes of composites containing different amounts of BaTiO₃.

Sample code	wt% BaTiO ₃	Sample code	wt% BaTiO ₃
P	0	P_5B	5
P_0.5B	0.5	P_7.5B	7.5
P_0.75B	0.75	P_10B	10
P_1B	1	P_30B	30
P_2.5B	2.5		

The dielectric constant variation is given in Fig. 6. To fit the axis labels, the codes given in Table II were used in Fig. 6. Since all samples were cured at 100°C for 35 min, only the constituent ratios were indicated in the codes. The ratios in front of B refer to the wt% BaTiO₃ mixed with PDMS. For example, P_2.5B means that PDMS contains 2.5 wt% BaTiO₃ nanoparticles in it. As shown in the graph, the dots represent the average dielectric constant values. There is an increase in dielectric constant until 1 wt% of BaTiO₃. After this value, there is a significant decrease with increasing BaTiO₃ content. According to the literature on nanomaterials, there is a percolation threshold which is around 1 wt%. After this percolation threshold — for some reason — properties begin to decrease [31]. For our research, this percolation threshold is obviously observable for dielectric constant.

The BaTiO₃ particles in P-1B sample are shown in Fig. 7. Because of the very small amount of weight percentage, there are few particles in the image in high magnification (×10k). Moreover, there are cracks on the surface which are the result of the nature of a low polymer matrix-filler interaction between PDMS and BaTiO₃ particles. This, in fact, is in contrast to the case of the 100C_35min PDMS sample shown in Fig. 4d. Nayak et al. explained

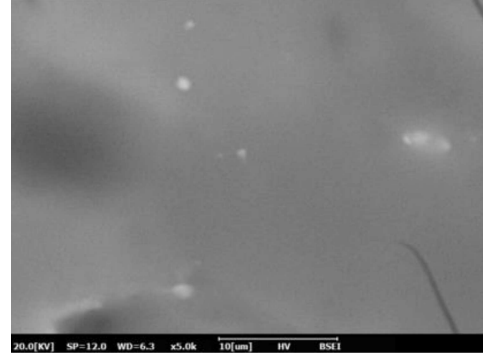


Fig. 7. SEM image of the sample cured at 100°C during 35 min and containing 1 wt% BaTiO₃.

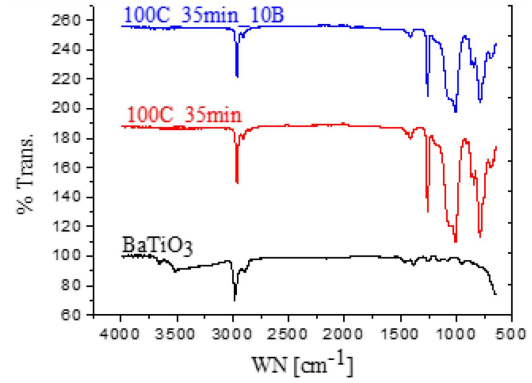


Fig. 8. Comparable FTIR data graph to observe BaTiO₃ effect on the bond properties.

this relation with the Kraus plot. The Kraus plot is a ratio between the volume fraction ratios of elastomer and filler as shown below

$$\frac{V_{r0}}{V_{rf}} = 1 - m \frac{\phi}{1 - \phi}, \quad (1)$$

where V_{r0} and V_{rf} are the elastomer volume fractions which belong to elastomers having different vulcanized procedures, ϕ is the filler volume fraction and m is the polymer-filler interaction parameter coming from the slope of V_{r0}/V_{rf} over $\phi/(1-\phi)$ [32].

According to this formula, a positive slope of this ratio gives a low polymer-filler interaction, meaning a non-reinforcing nature of the filler [32]. Therefore, the reason for crack formation in Fig. 7 is that by adding BaTiO₃ particles into the PDMS matrix, the elasticity of the silicon rubber decreases [12, 13, 33, 34].

To examine the effect of BaTiO₃ on the bonding properties in the PDMS, FTIR analyses were made. The comparable FTIR data belonging to BaTiO₃, the 100C_35min and 100C_35min_10B samples, are given in Fig. 8. There is no observable effect of BaTiO₃ on the bonding properties because of the dominant peaks of PDMS. The peak at around 3600 cm⁻¹ which belongs to BaTiO₃ is related with the O-H bonds coming from the moisture content at the surface of BaTiO₃ particles [18].

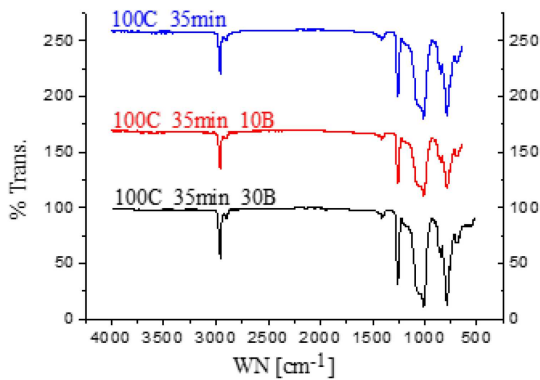


Fig. 9. Comparable FTIR data graph to observe the amount of BaTiO₃ effect on the bond properties.

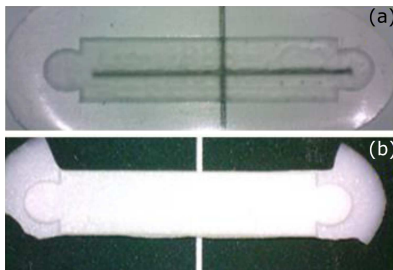


Fig. 10. (a) Pure PDMS, (b) PDMS with BaTiO₃ nanoparticle addition.

In Fig. 9, to observe the effect of BaTiO₃ content, the 100C_35min, 100C_35min_10B and 100C_35min_30B samples were compared. As it is seen, for the sample containing 10 wt% BaTiO₃, the transmittance between 1500 and 1000 cm⁻¹ wavelength decreased. For 30 wt% BaTiO₃, the transmittance values slightly increased. With the increase of additives in the PDMS matrix, the volume reacting with the infrared light decreased. Therefore, the infrared light could have reacted on a smaller volume of PDMS and the transmittance could have been higher than it should be. Another possibility is that because of the agglomeration, the particle size could have increased and, therefore, the intensity of the peak of 30 wt% BaTiO₃ containing the composite could have increased too [35]. Additionally, in Fig. 9 the peak at ≈ 1300 cm⁻¹ is shifted to the left by increasing the BaTiO₃ content [36].

In Fig. 10, the pure PDMS and the PDMS/BaTiO₃ composite digital microscope images are shown. As represented in the FTIR results, by the addition of BaTiO₃ nanoparticles, the composite gets opaque and its transmittance decreases.

4. Conclusions

In this study, we produced an EAP from a PDMS composite structure. Within the carried experimental studies, an optimum curing condition was adjusted as 100°C for 35 min. The highest dielectric

constant, namely 5.09×10^{-25} , was calculated with a crack-free surface. During the optimization of PDMS, curing conditions have not affected the molecular structure of PDMS according to results of the FTIR analyses.

To develop dielectric properties of a PDMS-based EAP, several BaTiO₃ ratios were mixed with PDMS to form a PDMS/BaTiO₃ nanocomposite. By increasing the BaTiO₃ content, the dielectric constant increased until 1 wt% and then it began to decrease. This is related with the percolation threshold values described in the literature mentioned in Sect. 3 of this paper. The transmittance values of BaTiO₃ and the PDMS overlapped because of the highly dominant nature of PDMS and very little amount of BaTiO₃ in it, according to FTIR. By increasing the BaTiO₃ content in the PDMS matrix, the peak values measured by FTIR were shifted to the left and their intensities increased due to the increase in the particle size caused by agglomeration.

Acknowledgments

This study was supported by the Scientific Research Project Unit of Dokuz Eylül University (project No. 2018.KB.FEN.025).

References

- [1] J.D.W. Madden, N.A. Vandesteeg, P.A. Anquetil, P.G.A. Madden, A. Takshi, R.Z. Pytel, S.R. Lafontaine, P.A. Wieringa, I.W. Hunter, *IEEE J. Ocean. Eng.* **29**, 706 (2003).
- [2] C.M. de Oliveira Ribeiro, Ph.D. thesis, Universidade do Minho, 2012.
- [3] R. Shankar, T.K. Ghosh, R.J. Spontak, *Soft Matter* **3**, 1116 (2007).
- [4] R. Shankar, T.K. Ghosh, R.J. Spontak, *Sens. Actuat. A Phys.* **151**, 46 (2009).
- [5] V. Finkenstadt, J.L. Willett, *Macromol. Symp.* **227**, 367 (2005).
- [6] Y. Bar-Cohen, *Expert Rev. Med. Dev.* **6**, 731 (2005).
- [7] R. Pelrine, R. Kornbluh, Q. Pei, J. Joseph, *Science* **287**, 836 (2000).
- [8] K. Ren, Ph.D. thesis, The Pennsylvania State University, 2007.
- [9] R.D. Kornbluh, R. Pelrine, J. Joseph, R. Heydt, Qibing Pei, in: *Proc. SPIE Conf. on Electroactive Polymer Actuators and Devices*, 1999, p. 149.
- [10] Z.Y. Cheng, V. Bharti, T.-B. Xu, Haisheng Xu, T. Mai, Q.M. Zhang, *Sens. Actuat. A Phys.* **90**, 138 (2001).
- [11] S.-H. Xie, B.-K. Zhu, X.-Z. Wei, Z.-K. Xu, Y.-Y. Xu, *Composites A* **36**, 1152 (2005).

- [12] A. Bele, G. Stiubianu, C.D. Varganici, M. Ignat, M. Cazacu, *J. Mater. Sci.* **50**, 6822 (2015).
- [13] S. Nayak, T.K. Chaki, D. Khastgir, *Adv. Mater. Res.* **622-623**, 897 (2013).
- [14] U. Yaqoob, G.S. Chung, *J. Alloys Compd.* **695**, 1231 (2017).
- [15] E.A. Stefanescu, X. Tan, Z. Lin, N. Bowler, M.R. Kessler, *Polymer (Guildf)*. **52**, 2016 (2011).
- [16] W. Choi, K. Choi, G. Yang, J.C. Kim, C. Yu, *Polym. Test.* **53**, 143 (2016).
- [17] M. Acosta, N. Novak, V. Rojas, S. Patel, R. Vaish, J. Koruza, G.A. Rosetti Jr., J. Rödel, *Appl. Phys. Rev.* **4**, 041305 (2017).
- [18] A. Moghtada, R. Ashiri, *Ultrason. Sonochem.* **33**, 141 (2016).
- [19] W.-S. Cho, E. Hamada, *J. Alloys Compd.* **266**, 118 (1998).
- [20] Y.S. Malghe, A.V. Gurjar, S.R. Dharwadkar, *Bull. Mater. Sci.* **27**, 217 (2004).
- [21] J. Lee, J. Kim, H. Kim, Young Min Bae, Kyeong-Hee Lee, Hyoung J. Cho, *J. Micromech. Microeng.* **23**, 035007 (2013).
- [22] A. Groza, A. Surmeian, *J. Nanomater.* **2015**, 204296 (2015).
- [23] Dow Corning, SYLGARD™ 184 Silicone Elastomer Kit Technical Data Sheet, 2013.
- [24] B.Ş. Akdemir, M.Sc. thesis, Dokuz Eylül University, 2019.
- [25] M.H. Madsen, N.A. Feidenhans'l, P.E. Hansen, J. Garnés, K. Dirscherl, *J. Micromech. Microeng.* **24**, 127002 (2014).
- [26] S.W. Lee, S.S. Lee, *Microsyst. Technol.* **14**, 205 (2008).
- [27] H. Schmid, B. Michel, *Macromolecules* **33**, 3042 (2000).
- [28] C. Moraes, Y. Sun, C.A. Simmons, *J. Micromech. Microeng.* **19**, 065015 (2009).
- [29] H. Wu, T.W. Odom, D.T. Chiu, G.M. Whitesides, *J. Am. Chem. Soc.* **125**, 554 (2003).
- [30] D. Prastiyanto, Ph.D. thesis, Karlsruhe Institute of Technology, 2015.
- [31] L. Chen, L. Lu, D. Wu, G. Chen, *Polym. Compos.* **28**, 493 (2007).
- [32] S. Nayak, T.K. Chaki, D. Khastgir, *ACS Publ.* **53**, 14982 (2014).
- [33] A. Bele, M. Cazacu, G. Stiubianu, S. Vlad, M. Ignat, *Composites B Eng.* **68**, 237 (2015).
- [34] A. Bele, M. Cazacu, G. Stiubianu, S. Vlad, *R. Soc. Chem. Adv.* **4**, 58522 (2014).
- [35] S. Kurien, Ph.D. thesis, Mahatma Gandhi University, 2005.
- [36] K.M. Proctor, M.Sc. thesis, Oklahoma State University, 1956.